

Author Manuscript

Title: How Second Coordination Sphere Modifications Can Impact Metal Structures in Proteins: A Crystallographic Evaluation

Authors: Vincent Louis Pecoraro; Leela Ruckthong, Ph.D.; Jeanne A. Stuckey, Ph.D.

This is the author manuscript accepted for publication and has undergone full peer review but has not been through the copyediting, typesetting, pagination and proofreading process, which may lead to differences between this version and the Version of Record.

To be cited as: 10.1002/chem.201806040

Link to VoR: <https://doi.org/10.1002/chem.201806040>

How Outer Coordination Sphere Modifications Can Impact Metal Structures in Proteins: A Crystallographic Evaluation

Leela Ruckthong^{1,2}, Jeanne A. Stuckey^{3,4} and Vincent L. Pecoraro^{1*}

¹Department of Chemistry, University of Michigan, Ann Arbor, Michigan 48109, USA

²Department of Chemistry, Faculty of Science, King Mongkut's University of Technology, Thonburi (KMUTT), Bang Mod, Thung Khru, Bangkok, 10140, Thailand

³Life Sciences Institute, University of Michigan, Ann Arbor, Michigan 48109, USA

⁴Department of Biological Chemistry, University of Michigan, Ann Arbor, Michigan 48109, USA

*e-mail: vlpec@umich.edu

Abstract: A challenging objective of *de Novo* metalloprotein design is to control of the outer coordination spheres of an active site to fine tune metal properties. The well-defined three stranded coiled coils, TRI and CoilSer peptides, are used to address this question. Substitution of Cys for Leu yields a thiophilic site within the core. Metals such as Hg(II), Pb(II) and As(III) result in trigonal planar or trigonal pyramidal geometries; however, spectroscopic studies showed Cd(II) formed 3-, 4- or 5-coordinate Cd(II)S₃(OH₂)_x (where x=0-2) when the outer coordination spheres were perturbed. Unfortunately, there has been little crystallographic examination of these proteins to explain the observations. Herein, we compare the high-resolution x-ray structures of apo- and mercaptated proteins to explain the modifications that lead to metal coordination number and geometry variation. It reveals that Ala substitution for Leu opens a cavity above the Cys site allowing for water excess, facilitating Cd(II)S₃(OH₂). Replacement of Cys by Pen restricts thiol rotation, causing a shift in the metal binding plane that displaces water, forming Cd(II)S₃. D-Leu, above the Cys site, reorients the side chain towards the Cys layer diminishing the space for water accommodation yielding Cd(II)S₃, while D-Leu below opens more space, allowing for equal Cd(II)S₃(OH₂) and Cd(II)S₃(OH₂)₂. These studies provide insights on how to control desired metal geometries in metalloproteins using coded and non-coded amino acids.

Keywords: *De novo* protein engineering, D-amino acids, Non-natural amino acids, Metalloprotein Engineering

Introduction

We have employed *de novo* designed proteins containing thiol residues to chelate metals in geometries that are relevant for understanding heavy metal sequestration in sulfur rich sites of human chaperones and metalloregulator proteins.¹⁻¹⁰ Using the TRI-family peptides (sequences given in **Table 1**) we have established a well-defined scaffold using three-stranded coiled coil (3SCC) forming peptides that can evaluate metal binding within a hydrophobic core (**Figure 1**). These peptides are based on a heptad repeat approach in which hydrophobic leucine (Leu) residues at **a** and **d** positions generate the helical core and salt bridge interactions between **e** and **g** residues on the helical interface stabilize the aggregation state and a parallel orientation of helices.¹⁰⁻¹² The substitution of Leu with cysteine (Cys) in one of the hydrophobic **a** or **d** positions generates a layer of three Cys residues forming a tri-sulfur chelating site. Previous reports have shown that the cysteine side chains in these apo-proteins are *preorganized* for binding metals into trigonal pyramidal geometries (i.e. Pb(II)S₃ and As(III)S₃), but are simply *predisposed* for encapsulating metals that are trigonal planar or pseudo-tetrahedral.¹³ In the preorganized systems, the ligands in the unbound state, which are directed toward the N-termini and helical core, remain almost in the same position upon metal

complexation. This is mainly because trigonal pyramidal geometry does not require the metal to bind in the same plane as the Cys sulfur atoms, but rather it may achieve the necessary bond lengths and angles when it is situated below the plane of coordinating atoms. However, *predisposition* of Cys occurs when the metal binding side-chains must rotate away from the helical core toward the helical interface, in order to increase space for metal binding within (Hg(II)) or close to (Zn(II)) the Cys plane. Since Cd(II) in a Cd(II)S₃ environment most likely binds into a geometry similar to trigonal planar Hg(II) rather than trigonal pyramidal Pb(II)^{14,15}, it is likely that Cys residues are predisposed rather than pre-organized toward trigonal planar Cd(II) sites in 3SCCs.

We have paid specific attention to Cd(II) binding to the TRI-family peptides to understand coordination number control in α -helical systems.¹⁻¹⁰ ¹¹³Cd NMR, ^{111m}Cd PAC, X-ray Absorption and UV-vis spectroscopies demonstrated that the incorporation of Cd(II) to the (TRIL16C)₃ peptide generated a mixture of trigonal planar Cd(II)S₃ and pseudo-tetrahedral Cd(II)S₃(H₂O).^{6-8,16-23} Unlike Hg(II), which prefers linear or trigonal planar structures, Cd(II) easily accepts 4-coordination when an exogenous ligand is available. The evidence for the formation of a Cd(II)S₃(H₂O) clearly implies that Leu residues in the twelfth position provide a certain amount of space that allows water

Table 1. Peptide sequences

Peptides		a b c d e f g	a b c d e f g	a b c d e f g	a b c d e f g	a b c d e f g	PDB ID
		2	9 12	16 19	23	30	
TRI	Ac-G	LKALEEK	LKALEEK	LKALEEK	LKALEEK	G-NH ₂	
TRIL16C	Ac-G	LKALEEK	LKALEEK	<u>C</u> KALEEK	LKALEEK	G-NH ₂	
TRIL12AL16C	Ac-G	LKALEEK	LKA <u>A</u> EK	<u>C</u> KALEEK	LKALEEK	G-NH ₂	
TRIL12 _D LL16C	Ac-G	LKALEEK	LKA <u>D</u> EK	<u>C</u> KALEEK	LKALEEK	G-NH ₂	
TRIL2WL16CL19 _D L	Ac-G	WKALEEK	LKALEEK	<u>C</u> KA <u>D</u> EK	LKALEEK	G-NH ₂	
CoilSer (CS)	Ac-E	WEALEKK	LAALESK	LQALEKK	LEALEHG	-NH ₂	
CSL16C	Ac-E	WEALEKK	LAALESK	<u>C</u> QALEKK	LEALEHG	-NH ₂	5K92 ¹³
CSL9PenL23H	Ac-E	WEALEKK	<u>Pen</u> ALESK	LQALEKK	HEALEHG	-NH ₂	3PBJ ²⁸
GRAND-CoilSer (GRAND-CS)	Ac-E	WEALEKK	LAALESK	LQALEKK	LQALEKK	LEALEHG -NH ₂	
GRAND-CSL16CL30H	Ac-E	WEALEKK	LAALESK	<u>C</u> QALEKK	LQALEKK	<u>H</u> EAL <u>E</u> HG-NH ₂	5KB0 ¹³ , 5KB1 ¹³
GRAND-CSL12AL16C	Ac-E	WEALEKK	LAA <u>A</u> ESK	<u>C</u> QALEKK	LQALEKK	LEALEHG-NH ₂	5KB2 ¹³ , 6EGO*
GRAND-CSL12 _D LL16C	Ac-E	WEALEKK	LAA <u>D</u> LESK	<u>C</u> QALEKK	LQALEKK	LEALEHG -NH ₂	6EGL*
GRAND-CSL16CL19 _D L	Ac-E	WEALEKK	LAALESK	<u>C</u> QA <u>D</u> LEKK	LQALEKK	LEALEHG -NH ₂	6EGM*, 6EGN*
GRAND-CSL12 _D LL16CL19 _D L	Ac-E	WEALEKK	LAA <u>D</u> LESK	<u>C</u> QA <u>D</u> LEKK	LQALEKK	LEALEHG -NH ₂	

Bold and underlined residues indicate substitutions.

N- and C-termini are capped by Ac and NH₂ groups, respectively.

* This work

access above the metal site, allowing the Cd(II) site to have bound water 60% of the time. However, when the sterics were altered by replacing Leu with alanine (Ala), TRIL12AL16C gave 100% Cd(II)S₃(H₂O).^{16,17} An exclusive trigonal planar Cd(II)S₃ could be formed with two strategies. First, a more sterically demanding analogue of Cys (β -dimethyl cysteine also called penicillamine (Pen)) was incorporated in lieu of Leu in the sixteenth position.^{12,16} The Cd(II)(TRIL16Pen)₃⁻ formed 100% Cd(II)S₃. Second, when the chirality of Leu in the twelfth position is inverted to D-Leu (TRIL12_DLL16C)²⁴ the branched side chain was proposed to reorient toward the C-termini of the 3SCC to block the space above the metal site. As predicted, a 100% Cd(II)S₃ was achieved. Based on this observation, the alternate configuration of D-Leu has been varied in the outer coordination spheres around the metal center to investigate how the coordination numbers of Cd(II) can be controlled. Based on ¹¹³Cd NMR and ^{111m}Cd PAC, the replacement of L-Leu by D-Leu at the nineteenth position (TRIL2WL16CL19_DL) led to Cd(II)S₃(H₂O) and Cd(II)S₃(H₂O)₂ in a percentage ratio of 50:50.²⁵ The evidence of this new Cd(II)S₃(H₂O)₂ species suggested that D-Leu potentially opens space below the metal site, thus the (TRIL2WL16CL19_DL)₃ contains two possible cavities both above and below the metal site at the same time. The incorporation of two D-Leu simultaneously above and below the metal site in the GRAND-CSL12_DLL16CL19_DL design, reduced the amount of Cd(II)S₃(H₂O)₂ by 20%, while the Cd(II)S₃(H₂O) species increases to 70%.²⁵ D-Leu obviously shows potential to engineer the steric environments that affects the availability of space around the metal center, which consequently controls water access around the metal site. Despite the success in ¹¹³Cd NMR and ^{111m}Cd PAC characterizations of this Cd(II)-bound peptide series, structural details of such modifications have not yet been revealed.

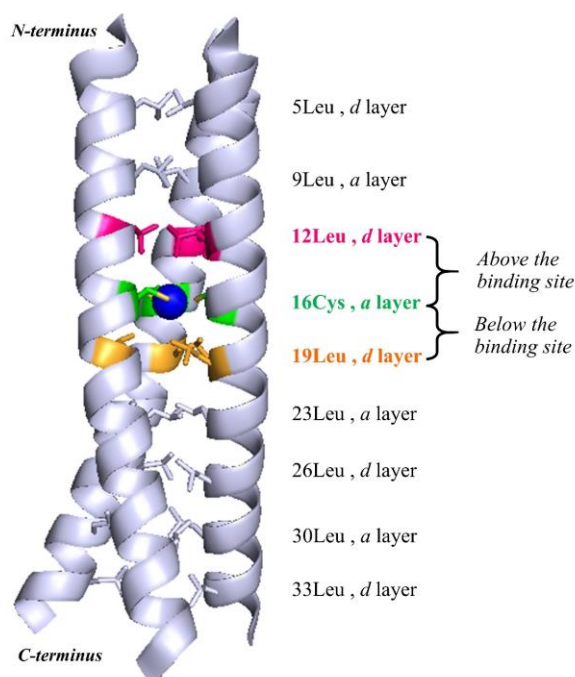
We have employed 3SCC CoilSer (CS) and GRAND-CoilSer (GRAND-CS) (Table 1) to act as crystallographic analogues in structural studies of these designs.^{11-13,21,22} Both peptides, differ by length, and contain a histidine (His) at the f position of the last heptad. This His located on the helical interface is critical for crystallization as it ligates to a Zn(II) ion along with glutamates from other trimers. The external Zn(II) sites facilitate the 3D

packing of trimers in lattice form. Spectroscopic studies have shown that the substitution of Leu with Cys in these

crystallographic analogues results in identical heavy metal binding properties as the TRI-family peptides.²² A number of X-ray crystallographic structures in both apo- and metallated forms of these peptides have been reported.^{11-13,23-24} Unfortunately, even though great effort has been spent on optimizing the crystal growth conditions of the designs, to date no crystal structures of CS or GRAND-CS constructs have been isolated with bound Cd(II). We believe that Cd(II) was unable to bind to the protein under the crystal growth conditions due to the high affinity of this metal ion toward the oxygen-containing precipitants that are present (e.g. polyethylene glycol, glycerol and ethoxyethanol). Usually these materials are at concentrations much higher than the protein, so it is likely that the Cd(II)-thiolate center cannot compete successfully for the metal in the presence of these concentrated oxygen ligands. Thus, direct observation of the Cd(II) within these 3SCCs under crystallization conditions has been unsuccessful.

To still be able to gain insight for the impact of modifying outer coordination sphere hydrophobic residues, we have utilized Hg(II) to represent a trigonal planar Cd(II). The Hg(II)-S bond distance in Hg(II)₃Zn(II)_N(GRAND-CSL16CL30H)₃⁺ crystal structure (PDB ID: 5KB1) was reported to be 2.38 Å¹³, which is in good agreement with an X-ray absorption result for Hg(II)(TRIL16C)₃⁻ (2.43 Å).⁷ At the same time, the EXAFS results for the Cd(II)-S bond distance for the trigonal planar Cd(II)(TRIL16Pen)₃⁻ is 2.46 Å,²⁹ which leads one to predict the trigonal planar structures of Hg(II)S₃ and Cd(II)S₃ are similar. Thus, regardless of the metal size difference, the crystallographic Hg(II)S₃ structures could be used to explain general characteristics of Cd(II)S₃. In this study, we have also achieved a variety of crystal structures based on the sequences designed for Cd(II) studies. We have obtained the Hg(II)(GRAND-CSL12AL16C)₃⁻, representing the TRIL12AL16C environment, to analyze the effect of Ala (twelfth position) above the metal site in comparison with the 12Leu packing of the known Hg(II)₃Zn(II)_N(GRAND-CSL16CL30H)₃⁺.¹³ The analysis will explain why Cd(II)(TRIL16C)₃⁻ can form a mixture of Cd(II)S₃ and Cd(II)S₃(H₂O) centers, whereas Cd(II)(TRIL12A16C)₃⁻ results in a 100% Cd(II)S₃O. Moreover, the exclusion of water from the Pen₃ site has been investigated using a combination

between $\text{Hg(II)}_3\text{Zn(II)}_3(\text{GRAND-CSL16CL30H})_3^+$ and $[\text{Hg(II)}]_3[\text{Zn(II)}]$ ($\text{H}_2\text{O}/\text{OH}^-$)



$)]_3(\text{CSL9PenL23H})_3^{\text{nt}}$. We have crystallized apo-(GRAND-CSL12_DLL16C)₃ and apo-(GRAND-CSL16CL19_DL)₃ to

Figure 1. General overview of GRAND-CS structure that contains a $\text{Hg(II)}_3\text{S}_3$ binding site at the sixteenth position. Helical core residues are shown as sticks. Leucine residues in the 12th and 19th positions are shown in pink and orange, respectively. Cys residues in the 16th position are colored green. Hg(II) is shown as a blue sphere. The Leu layer at the 12th position and the interlayer between the 12th and 16th positions are defined as 'above' the metal binding site. The Leu layer at the 19th position and the interlayer between the 16th and 19th positions are defined as 'below' the metal binding site.

investigate the steric interference caused by D-Leu. Additionally, the metalated $\text{Hg(II)}(\text{GRAND-CSL16CL19}_D\text{L})_3^-$ structure is used to examine cavities around the metal site. This structural analysis explains how steric engineering can be applied to vary Cd(II) geometries from 3-, 4- to 5-coordinate around the metal site of 3SCCs. This knowledge is useful for biophysical applications when one would want to design a desired metal site in a protein to control coordination number or provide access for solvent or substrate in catalytic reactions.

Results and Discussion

The objective of these studies is to understand how outer coordination sphere residues influence coordination number on metals bound within the hydrophobic region of a 3SCC structure. These studies are not only interesting from a theoretical viewpoint, as they suggest strategies to control metal ion coordination number or substrate access to a metallo-catalytic

center in designed proteins, but also to elucidate factors that may define the stability of metal binding to native 3SCC regions as found in the ORF1p protein of the LINE-1 human retrotransposon, which also contains layers of cysteine thiolates within the hydrophobic core of a 3SCC domain.^{30–32}

In this section, we will address how changing the steric factors of side chain residues located toward the N-terminus (above the metal site), the C-terminus (below the metal site) or on the ligands themselves (Pen) influence the structure of the metal binding site. In general, while crystals using the parent TRI peptides can form, they diffract poorly as they are not ordered in one dimension. To resolve this problem, CS peptides (either CS or GRAND-CS which is one heptad longer leading to a more stable scaffold) have been examined. In all cases, the metal binding behaviors between TRI and CS derivatives are identical. While it is preferable to have completed these studies using the relevant Cd(II), crystals of CS derivatives with this ion have not been forthcoming. Therefore, we will use Hg(II) as an analogue of Cd(II) binding in trigonal planar and trigonal bipyramidal binding environments. This substitution is reasonable given that previous EXAFS analysis has shown that trigonal planar Cd(II) complex in these peptides have Cd(II)-S distances of 2.46 Å^{19,20}, while the Hg(II) structure exhibited Hg(II)-S of 2.38 Å.¹³

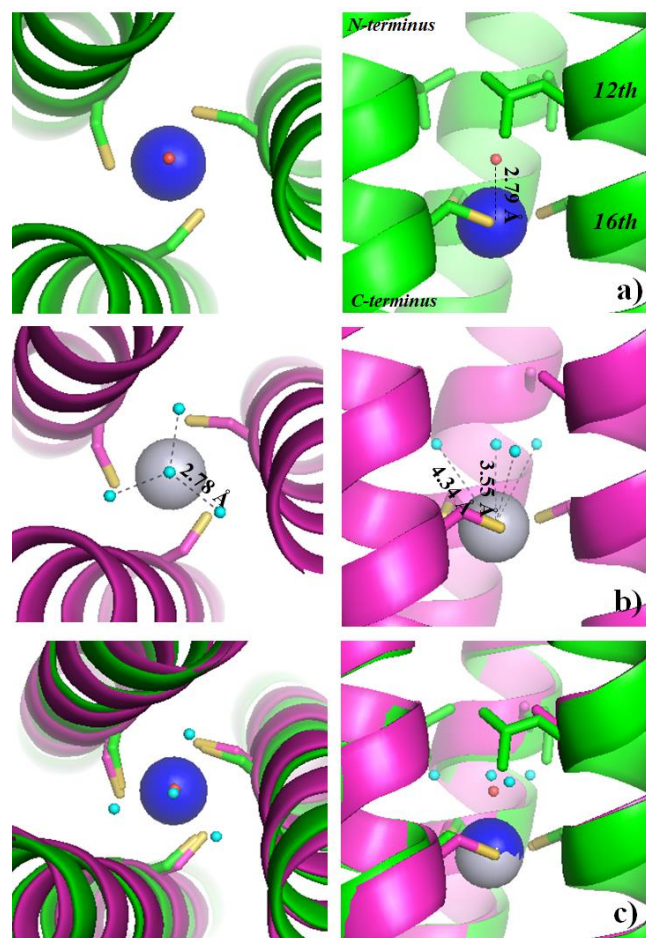
The parent peptide CSL16C binds Cd(II) with a 60:40 mixture of Cd(II)S₃(H₂O) and Cd(II)S₃. We will first discuss, why this ratio occurs when L-leucine residues are located above and below the sulfur metal binding plane. We will then explain how replacing L-Leu with L-Ala (GRAND-CSL12AL16C) provides an environment that allows isolation of a 100% Cd(II)S₃(H₂O). Following this discussion we will explain how two alternative methods, replacing cysteine by Pen (CSL16Pen) or altering the chirality of the Leu above the cysteine layer (GRAND-CSL12_DLL16C), constrict the metal environment to give exclusively Cd(II)S₃. Finally, we will show how alteration of chirality below the sulfur plane allows greater access to solvent, ultimately leading to a structure that has a significant degree of Cd(II)S₃(H₂O)₂ species. These studies demonstrate how altering chirality around the metal binding site can enhance or diminish solvent access, depending on the placement of the substitution.

Allowing 4-coordinate Cd(II) by Removal of Steric Bulk: Leu to Ala Mutation

Modifications of residues in outer coordination spheres play an important role in modulating solvent access to the metal-binding site, as well as metal site hydration and metal ion coordination.^{33–36} Unlike Leu, Ala contains a single methyl group (C_β carbon) attached to the α-carbon. Alber *et al.* had shown that conversion of Leu to Ala allowed for the addition of four waters into the cavity generated in 4-helix bundles by removing the leucine isopropyl groups.³⁶ Though the 3SCC is a narrower construct, it might be expected to behave similarly. Lee *et al.* substituted Ala for the more bulky Leu at the twelfth position to provide a water pocket above the metal site in (TRIL12AL16C)₃.^{16,17} The design resulted in an exclusive 100% Cd(II)S₃(H₂O).^{16,17} While a structure of Cd(II)(CSL12AL16C)₃⁻ has not been obtained, structural understanding of the design

can still be achieved using the related $\text{Hg(II)(GRAND-CSL12A16C)}_3^-$.

To see the effect of 12Ala compared to 12Leu, the $\text{Hg(II)(GRAND-CSL12A16C)}_3^-$ structure is overlaid onto the known $\text{Hg(II)}_5\text{Zn(II)}_N(\text{GRAND-CSL16CL30H})_3^+$ (**Figure 2**). In both cases, Hg(II) is found as a trigonal planar structure. Previous work has shown the GRAND-CS peptides are predisposed to bind trigonal planar or pseudo-tetrahedral metals¹³, meaning that a large rotation of the thiol from the apo-protein is required upon metal complexation. In trigonal planar structures, Hg(II) induces $\sim 100^\circ$ of apo-Cys rotation from a position pointing upward toward the N-termini to being directed downward toward the C-terminal end. This rotamer reorientation expands the hydrophobic cavity above the sulfur plane sufficiently to accommodate a water molecule as seen in $\text{Hg(II)}_5\text{Zn(II)}_N(\text{GRAND-CSL16CL30H})_3^+$.¹³ The three Cys residues in $\text{Hg(II)(GRAND-CSL12A16C)}_3^-$ are symmetric due to crystallographic requirements of the R32 space group. Each Cys contains two rotamers (**Figure S1**) in which only the major conformer is suitable to bind the metal with an orientation toward the helical interface ($\chi_1 = -150.92^\circ$). This χ_1 value is close to the -150.35° observed in $\text{Hg(II)}_5\text{Zn(II)}_N(\text{GRAND-CSL16CL30H})_3^+$ indicating that the orientations of the bound Cys ligands in both structures are similar (**Figure 2c**). Such arrangements make the metal pocket sizes comparable (S_7-S_7 separation of 4.24 Å for $\text{Hg(II)(GRAND-CSL12A16C)}_3^-$ and 4.08 Å for $\text{Hg(II)}_5\text{Zn(II)}_N(\text{GRAND-CSL16CL30H})_3^+$). The Hg(II) ion in $\text{Hg(II)(GRAND-CSL12A16C)}_3^-$ is situated at a distance of 0.26 Å below the 16Cys plane with an averaged Hg(II)-S distance of 2.44 Å and average S-Hg(II)-S angle of 118.21° (**Table 3**). These values correspond closely to those observed in $\text{Hg(II)}_5\text{Zn(II)}_N(\text{GRAND-CSL16CL30H})_3^+$. Taken together these parameters confirm that both designs show essentially identical first coordination environments for $\text{Hg(II)}S_3$. Moreover, the apo-protein is also predisposed for Hg(II) binding in $\text{Hg(II)(GRAND-CSL12A16C)}_3^-$ (**Figure S2**). These indicate that a trigonal planar $\text{Cd(II)}S_3$ is not restricted from forming in the 12Leu peptide. Therefore, we can expect that the change in the $\text{Cd(II)}S_3(\text{H}_2\text{O})$ to $\text{Cd(II)}S_3$ ratio is not a consequence of the first coordination sphere, but rather depends on factors associated with the outer coordination spheres that surround the metal pocket. **Figure 3** emphasizes the steric hindrance generated from the aliphatic isobutyl side chain of Leu compared to the methyl group of Ala. It is obvious that Ala generates a hole above the metal site confirming the proposed impact of the modification. As a consequence, the larger space in $\text{Hg(II)(GRAND-CSL12A16C)}_3^-$ allows for up to four waters to access the metal binding site (**Figure 2b**). This observation is consistent with Alber's previous study³¹, providing a convenient explanation for the shift in coordination mode to fully $\text{Cd(II)}S_3(\text{H}_2\text{O})$. In contrast, in $\text{Hg(II)}_5\text{Zn(II)}_N(\text{GRAND-CSL16CL30H})_3^+$, only a single, unbound water that sits on the threefold axis directly above the metal at a 2.79 Å distance is observed (**Figure 2a**). In $\text{Hg(II)(GRAND-CSL12A16C)}_3^-$, one of the waters behaves in the same way as the observed water in the 12Leu-structure. Indeed, it is again located



on a threefold axis at a non-bonding distance of 3.55 Å from Hg(II) (**Figure 2b**). Moreover, the other three waters are threefold related, but located close to the helical interface between two neighbouring strands with a distance of 4.34 Å from the Hg(II) center. These waters form a hydrogen bonding network and are separated by a distance of 2.78 Å from the central water. Each solvent is found within the same plane (with respect to the N-termini). Such distances of Hg(II) to water are too long to be a Hg(II)-O bond (predicted to be ~ 2.20 Å), therefore, all of the waters found within the cavity are considered to be uncoordinated and stabilized through H-bonding interactions

Figure 2. Comparison of the $\text{Hg(II)}S_3$ sites and the amount of observed waters above the metal site between the $\text{Hg(II)}_5\text{Zn(II)}_N(\text{GRAND-CSL16CL30H})_3^+$ (PDB code: 5KB1)¹³ and $\text{Hg(II)(GRAND-CSL12A16C)}_3^-$. Left to right columns demonstrating top-down and side-on views of the Hg(II) binding sites in the sixteenth position. In a) $\text{Hg(II)}_5\text{Zn(II)}_N(\text{GRAND-CSL16CL30H})_3^+$, b) $\text{Hg(II)(GRAND-CSL12A16C)}_3^-$ and c) an overlay between the two structures. Main chain atoms of $\text{Hg(II)}_5\text{Zn(II)}_N(\text{GRAND-CSL16CL30H})_3^+$ and $\text{Hg(II)(GRAND-CSL12A16C)}_3^-$ are green and pink, respectively. 16Cys, 12Leu and 12Ala side-chains are shown as sticks (sulfurs=yellow). Hg(II) atoms in the $\text{Hg(II)}_5\text{Zn(II)}_N(\text{GRAND-CSL16CL30H})_3^+$ and $\text{Hg(II)(GRAND-CSL12A16C)}_3^-$ are present as blue and gray spheres, respectively. The observed waters in $\text{Hg(II)}_5\text{Zn(II)}_N(\text{GRAND-CSL16CL30H})_3^+$ and $\text{Hg(II)(GRAND-CSL12A16C)}_3^-$ are shown as small red and cyan spheres.

between each other and the backbone of peptides. Another compelling point to support the large size of the cavity formed

with 12Ala is the observation of a longer Hg(II) to the central water distance in Hg(II)(GRAND-CSL12A16C)₃⁻ (3.55 Å) than in Hg(II)₅Zn(II)_N(GRAND-CSL16CL30H)₃⁺ (2.79 Å). This increase in Hg(II)-O separation clearly demonstrates that more space is available in the 12Ala-containing structure for the water to move upward because it can form H-bonding to the additional three waters that also occupy in the cavity. The different number of water molecules between the two structures can explain the different degrees of solvation of Cd(II) between TRIL12A16C and TRIL16C designs. This observation proves that a cavity for solvent exists and it may allow for some water access when Cd(II) is bound to the metal site. Furthermore, EXAFS data indicate that

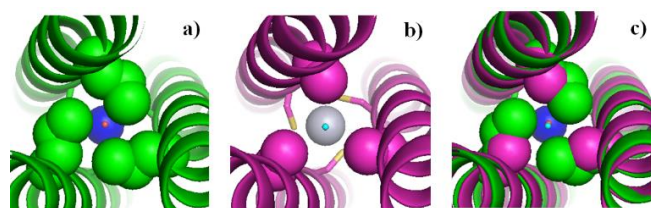


Figure 3. Packing of residues (shown as spheres) in the twelfth position above the metal site representing less hydrophobic character of Ala in Hg(II)(GRAND-CSL12AL16C)₃⁻ compared to Leu in Hg(II)₅Zn(II)_N(GRAND-CSL16CL30H)₃⁺ (PDB code: 5KB1)¹³. From top down view of the N-termini, a) 12Leu residues in the Hg(II)₅Zn(II)_N(GRAND-CSL16CL30H)₃⁺, and b) 12Ala residues in the Hg(II)(GRAND-CSL12AL16C)₃⁻. In c) an overlay between a) and b). Main chain atoms of Hg(II)₅Zn(II)_N(GRAND-CSL16CL30H)₃⁺ and Hg(II)(GRAND-CSL12AL16C)₃⁻ are shown in green and pink, respectively. Cys residues are shown as sticks (sulfurs=yellow). Hg(II) atoms in the Hg(II)₅Zn(II)_N(GRAND-CSL16CL30H)₃⁺ and Hg(II)(GRAND-CSL12AL16C)₃⁻ are present as blue and grey spheres, respectively. The observed waters in the Hg(II)₅Zn(II)_N(GRAND-CSL16CL30H)₃⁺ and Hg(II)(GRAND-CSL12AL16C)₃⁻ are shown as small red and cyan spheres

a Cd(II)-O bond in a Cd(II)S₃(H₂O) structure is 2.35 Å,¹⁹ which would appear achievable based on the Hg(II) to water separation in the crystal structures. However, one must remember that Hg(II) forms a trigonal planar structure whereas Cd(II) would have a 4-coordinate pseudo-tetrahedral polyhedron. This means that the Cd(II) would need to be displaced above the three sulfur atom plane toward the solvent ligand. As the spectroscopic data indicated that only 60% of Cd(II)S₃(H₂O) is present in Cd(II)(TRIL16C)₃⁻,⁷ this suggests that in a four coordinate structure the cavity may not be capable of stabilizing water well in the hydrophobic core. This is likely due to a combination of steric clashes between the bound water and the isobutyl side chains of leucine and the lack of additional hydrogen bonding atoms in close proximity that would stabilize the coordinated water. In the TRIL12AL16C design, this steric restriction is no longer operative, even for a four coordinate complex, and multiple waters that may H-bond to the bound water are present. Thus, Cd(II)S₃(H₂O) is the only species that forms in Cd(II)(TRIL12AL16C)₃⁻.

This structural analysis explains the factors that control the binding of water to Cd(II) in TRIL16C and TRIL12AL16C type peptides; however, equally interesting are the constraints that exclude water from the Cd(II) coordination environment to yield Cd(II)S₃ systems in other designed peptides.

Enforcing 3-coordinate Cd(II) Through Steric Interference of the Metal Binding Ligand: Cys to Pen Mutation

Lee *et al.* demonstrated that the incorporation of the Pen ligand in lieu of Cys at the sixteenth position (TRIL16Pen) led to Cd(II)S₃ coordination as confirmed by ¹¹³Cd NMR and ^{111m}Cd PAC spectroscopies.¹⁶ The spectroscopic evidence has been confirmed by structural analysis. Upon metal binding, the methyl groups prevent the thiol side chains from rotating downward toward the C-terminal end as observed for the L-cys derivative. Thus, the ligands stay in roughly the same position as in the apo protein indicating that Pen is highly preorganized for metal binding. The consequence of this modification is that the sulfur plane cannot shift toward the C-termini and must remain close to the Leu layer above the metal site (as compared to the Cys derivative). In this situation, the space above the Pen layer becomes insufficient for water accommodation. Consequently, the formation of Cd(II)S₃ is favorable in Cd(II)(CSL16Pen)₃.

Three possible explanations are considered for the perturbation of metal coordination environments by penicillamine. First, Pen ligands could have positioned their γ -methyl groups toward the space above the metal plane resulting in a smaller cavity above the site that excludes solvent access. Second, Pen might have undergone conformational changes upon metal complexation that excluded the water. Third, Pen ligands could have perturbed the primary coordination sphere of the metal in a specific way that encouraged a Cd(II)S₃ structure.

The first hypothesis was refuted by analysis of the aligned apo-(CSL16Pen)₃ (PDB ID: 3H5F)¹² and apo-(CSL16C)₃ (PDB ID: 5K92)¹³ structures. The helical backbones of the two structures are well-overlaid (RMSD = 0.17). The incorporation of Pen does not perturb the helical framework (**Supporting Information Figure S3, a**). Only the major conformers (with 95% occupancy) are considered to be oriented for metal binding as the thiols are directed into the helical core (**Supporting Information Figure S4, b**) which resembles the major Cys residues in apo-(CSL16C)₃, where the S _{γ} atoms point at the central core and toward the N-termini (**Supporting Information Figure S3, b and c**). The thiol pocket in the apo-(CSL16Pen)₃ (average S _{γ} -S _{γ} separation of 3.71 Å) is slightly larger than in the apo-(CSL16C)₃ (3.32 Å). While the S _{γ} atoms of Pen in apo-(CSL16Pen)₃ are oriented toward the interior of the coiled coil, the γ -methyl groups are pointing to the exterior. The fact that the Pen rotamers are almost at full occupancy (95%) suggests that these side-chain conformations are geometrically preferred when Pen is placed at the sixteenth position; however, the similar orientations of γ -thiols observed in the Cys structure exhibits only 70% occupancy, implying that there is more free rotation of γ -thiols in Cys rather than Pen. The rigidity of these S _{γ} angles in apo-(CSL16Pen)₃ likely results from the restricted thiol rotation around C _{β} atom due to the steric constraint imposed by the two γ -methyl groups of Pen. Based on these observations, the γ -methyl groups of Pen, which are oriented toward the helical interface, are not positioned to block the space above the metal site (between the 12Leu and 16Pen layers) that potentially excludes water from binding to Cd(II).

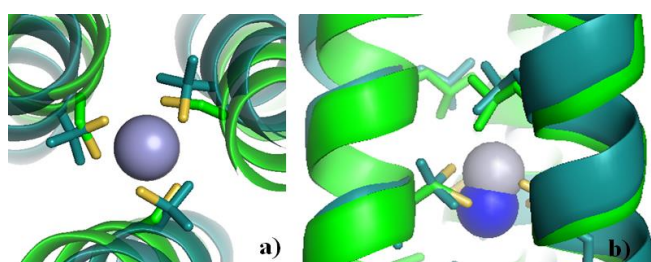


Figure 4. Comparison of the trigonal planar structures of Hg(II)(S-Cys)_3^- from $\text{Hg(II)}_5\text{Zn(II)}_N(\text{GRAND-CSL16CL30H})_3^+$ (PDB code: 5KB1)¹³ and Hg(II)(S-Pen)_3^- from the $[\text{Hg(II)}_5\text{Zn(II)(H}_2\text{O/OH}^-)]_N(\text{CSL9PenL23H})_3^{\text{nt}}$ (PDB code: 3PBJ)²⁸. a) Top-down from the N-termini and b) side-on views of the overlay. Main chain atoms of $\text{Hg(II)}_5\text{Zn(II)}_N(\text{GRAND-CSL16CL30H})_3^+$ are colored in green and $[\text{Hg(II)}_5\text{Zn(II)(H}_2\text{O/OH}^-)]_N(\text{CSL9PenL23H})_3^{\text{nt}}$ in cyan. Cys, Pen and Leu (above the metal site) are shown as sticks (sulfurs=yellow). Hg(II) atoms in the $\text{Hg(II)}_5\text{Zn(II)}_N(\text{GRAND-CSL16CL30H})_3^+$ and $[\text{Hg(II)}_5\text{Zn(II)(H}_2\text{O/OH}^-)]_N(\text{CSL9PenL23H})_3^{\text{nt}}$ are labelled as blue and grey spheres, respectively.

The second hypothesis can be dismissed by comparing the previously published structure of $[\text{Hg(II)}_5\text{Zn(II)(H}_2\text{O/OH}^-)]_N(\text{CSL9PenL23H})_3^{\text{nt}}$ with that of the apo-(CSL16Pen)₃ to reveal the behavior of trigonal planar Hg(II) binding to Pen-ligand in an a site. The $[\text{Hg(II)}_5\text{Zn(II)(H}_2\text{O/OH}^-)]_N(\text{CSL9PenL23H})_3^{\text{nt}}$ contains a trigonal planar Hg(II)(S-Pen)_3^- .²⁸ The bound Pen ligands (**Supporting Information Figure S5, b**) direct their S_γ atoms toward the interior core while positioning the γ-methyl groups out toward the helical interface. This S_γ configuration is similar to that observed in the apo-(CSL16Pen)₃ (**Supporting Information Figure S5, a**).¹² The invariance of the thiol layer between the non-metallated and metallated proteins can be underscored by their very tiny torsion angle shift (**Table 1**), that results in almost equal S_γ-S_γ separations between the two structures (3.71 versus 3.84 Å for apo-(Pen)₃ and Hg(II)(S-Pen)_3^- , respectively) (**Supporting Information Figure S5, c**). The highly similar sulfur planes emphasize that apo-Pen ligands exhibit a high degree of preorganization for metal binding, which could be due to the rigidity caused by the bulky γ-methyl substitution that prevents the γ-thiol from moving freely through space. Therefore, the second hypothesis that a conformational change of the Pen side chain is responsible for the presence of 100% Cd(II)S₃ structure appears to be incorrect.

The third hypothesis suggested a change in the first coordination sphere orientation that is imposed by the remote

Table 2: Crystallographic parameters observed from the crystal structures^a

Peptides	apo-(CSL16C) ₃ (PDB code: 5K92) ¹³	$\text{Hg(II)}_5\text{Zn(II)}_N(\text{GRAND-CSL16CL30H})_3^+$ (PDB code: 5KB1) ¹³	apo-(CSL16Pen) ₃ (PDB code: 3H5F) ¹²	$[\text{Hg(II)}_5\text{Zn(II)(H}_2\text{O/OH}^-)]_N(\text{CSL9PenL23H})_3^{\text{nt}}$ (PDB code: 3PBJ) ²⁸	$\text{Hg(II)}_5(\text{GRAND-CSL12A16C})_3^-$ (PDB code: 6EEO)	apo-(GRAND-CSL12eLL16C) ₃ (PDB code: 6EGL)	apo-(GRAND-CSL16CL19eL) ₃ (PDB code: 6EGM)	$\text{Hg(II)}_5(\text{GRAND-CSL16CL19eL})_3^-$ (PDB code: 6EGN)
16Cys rotamers								
χ ₁ (interior rotamers) ^b	-66.24° (average)	-150.35°	-49.85° (average)	-50.23° (average)	-150.92°	-68.57°	-61.13°	-153.11° (average)
S _γ -S _γ distance (Å) ^c	3.32 (average)	4.08	3.71 (average)	3.84 (average)	4.24	3.22	3.31	4.19 (average)
χ ₁ (exterior rotamers)	-176.47° (average) ^b	-169.58°	72.99° (average)	-	-56.73°	-174.79°	-	-28.85°, -94.80°
S _γ -S _γ distance (Å) ^c	5.33 (average)	5.06	8.45 (average)	-	3.24	5.93	-	3.66 (average)
Metal site								
M-S bond length (Å)	-	2.38, Hg(II)-S	-	2.23, Hg(II)-S (average)	2.44, Hg(II)-S	-	-	2.44, Hg(II)-S (average)
S-M-S angle (average)	-	118.50°	-	119.90°	118.21°	-	-	119.69°
Distance of metal from to the bound Cys plane (Å) ^d	-	-0.3	-	-0.06	-0.26	-	-	-0.12
Leu rotamers above the metal site	(12L-Leu)	(12L-Leu)	(12L-Leu)	(5L-Leu)		(12D-Leu)	(12L-Leu)	(12L-Leu)
Interior C _γ separation (Å) ^e	4.40	3.89	4.94	3.60	-	3.93	4.04	4.06
Exterior C _γ separation (Å) ^e	6.73	6.13	6.74	5.84	-	4.53	6.45	6.39
Distance of the layer from the interior sulfur plane (Å)	4.92	5.92	4.95	4.86	-	2.32	4.72	-6.17

methyl groups. This can be assessed by comparing the coordination spheres of the Hg(II)(S-Pen)_3^- and Hg(II)(S-Cys)_3^- in $[\text{Hg(II)}_5\text{Zn(II)(H}_2\text{O/OH}^-)]_N(\text{CSL9PenL23H})_3^{\text{nt}}$ and $\text{Hg(II)}_5\text{Zn(II)}_N(\text{GRAND-CSL16CL30H})_3^+$ (**Figure 4**). We observe that the thiol orientations of the bound-Cys and bound-Pen point

in completely opposite directions. While the Pen ligands are

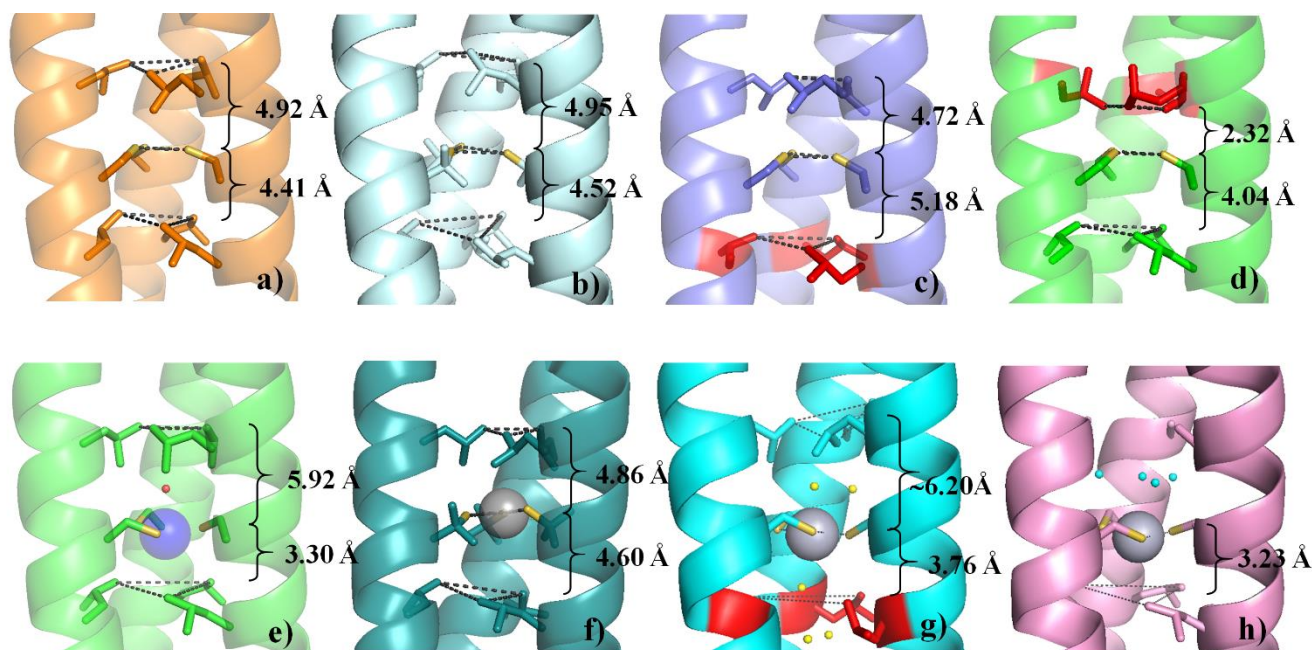
oriented to the interior of the 3SCC, the Cys residues instead are directed further out toward the helical interface as confirmed by the different χ₁ torsion angles of the two ligands [-49.85° observed in Hg(II)(S-Pen)_3^- and -150.35° in Hg(II)(S-Cys)_3^-] (**Figure 4a**). The average S_γ-S_γ separation in Pen is subsequently shorter than Cys by 0.24 Å, verifying that Cys can make a larger triangular metal plane compared to Pen. This observation indicates that the γ-methyl groups of Pen inhibit the expansion of the three atom sulfur plane to the requisite distances that are optimal for a trigonal Hg(II) species. The predisposed apo-Cys peptide reorients the γ-thiols downward toward the C-termini and facing out toward the helical interface in order to accept Hg(II) into the metal plane.¹³ The Hg(II)-Cys plane is shifted ~1.30 Å down toward the C-termini with respect to the apo-Cys structure¹³, whereas due to the preorganization of Pen ligands the sulfur plane is essentially unaltered on Hg(II) binding. **Figure 4b** illustrates the difference between the metallated planes in these proteins. The Hg(II)(S-Pen)_3^- is positioned about 1.80 Å more toward the N-termini relative to Hg(II)(S-Cys)_3^- . Clearly, the immobility of the Pen side chains requires the metal to bind in a more compressed trigonal plane that is located further toward the N-termini. Since the packing of the 12Leu layers remain unchanged between the Hg(II)(S-Cys)_3^- and Hg(II)(S-Pen)_3^- while the metallated-Pen plane is higher than in the bound-Cys form, there is a less space available for a fourth ligand in the Pen structure. **Supporting Information Figure S6 (top panels)** shows that the packing of the Leu residues above the Hg(II)(S-Pen)_3^- site is, in fact, slightly tighter than in the Hg(II)(S-Cys)_3^- . As a consequence, the Leu layer is at a distance of 4.86 Å from the bound-16Pen plane, whereas the related distance determined from the Hg(II)(S-Cys)_3^- lengthens to 5.92 Å (**Figure 5**). The impact of this difference in interlayer spacing on water access

Leu rotamers below the metal site	(19L-Leu)	(19L-Leu)	(19L-Leu)	(12L-Leu)	(19L-Leu)	(19L-Leu)	(19D-Leu)	(19D-Leu)
Interior C _β separation (Å)	4.64	6.17	5.86	5.28	6.47	5.30	5.17	8.09(average)
Exterior C _β separation (Å)	7.25	9.08	8.66	8.45	9.30	8.22	8.96	11.49(average)
Distance of the layer from the interior sulfur plane (Å)	4.41	3.30	4.52	4.60	3.23	4.04	5.18	3.76

^aPeptides that were crystallized in R32 space group have crystallographically imposed 3-fold symmetry along the z axis that runs through the center of the three helices of the 3SCC. The consequence of symmetry is that structures in R32 will have a single reported value for the following crystallographic parameters (χ_1 dihedral angles, atomic distances, and M-S distances), while average values are usually given for the structure crystallizing in C2 in which the three helices are independent. ^b χ_1 of Cys residue is determined from the dihedral angle of N-C_α-C_β-S_γ. ^cThe distance determined between S_γ atoms of the interior Cys conformers. ^dThe distance determined between S_γ atoms of the exterior Cys conformers. ^ePlus sign (+) indicates the metal is situated above the bound Cys plane. Minus (-) indicates the metal is situated below the bound Cys plane. ^fInterior C_β separation define the average distance between the interior C_β atoms of Leu residues of all chains. ^gExterior C_β separation define the average distance between the exterior C_β atoms of Leu residues of all chains. ^hAverage χ_1 dihedral angle determined from minor Cys conformers observed from two of the chains. ⁱAverage S_γ-S_γ separation determined from the two minor Cys conformations found on two chains and the third Cys (major) from the remaining chain. ^j χ_1 dihedral angle determined from minor Cys conformers observed from two chains.

is supported by the absence of a water molecule in **Enforcing 3-coordinate Cd(II) By Modification of Outer**

the area above the Pen-ligand binding site in the



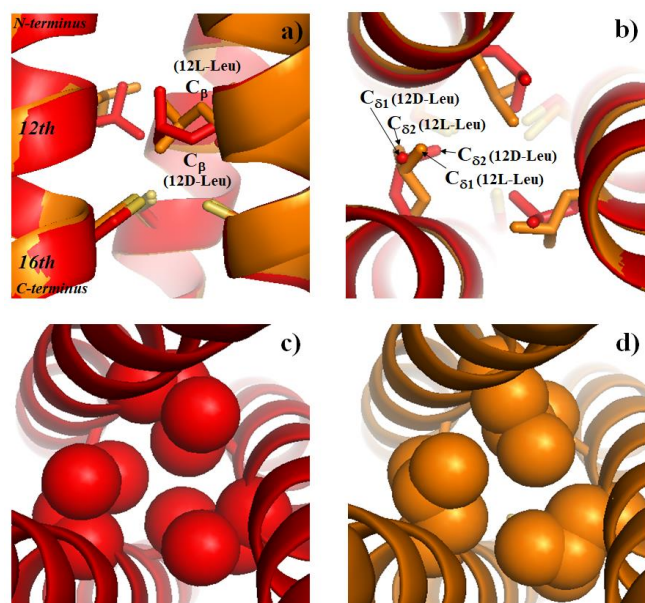
[Hg(II)]₃[Zn(II)(H₂O/OH)]₃(CSL9PenL23H)₃.²⁸ Moreover, the aligned binding sites (**Supporting Information Figure S6, bottom panel**) also show that the coordinated Hg(II) in Hg(II)(S_{Pen})₃ occupies the space where the water was previously observed in Hg(II)₃Zn(II)₃(GRAND-CSL16CL30H)₃⁺. It is obvious that Pen cannot generate enough space to accommodate a polar molecule within the hydrophobic core above the metal site. Therefore, these observations support the third formulated hypothesis.

The restriction of the metal binding S₃ plane in the presence of Pen ligands likely translates to the Cd(II) proteins. The shift of the metal plane toward the Leu residues and concurrent induction of a tighter hydrophobic packing above the metal site would act in concert to generate less space for solvents. This reasoning supports a model for complete water exclusion (full Cd(II)S₃ formation) in Cd(II)(TRIL16Pen)₃⁻. This hypothesis has been confirmed by the corresponding ¹¹³Cd NMR and ^{111m}Cd PAC results.¹⁶

Coordination Sphere Chirality: L-Leu to D-Leu Mutation on N-terminal Side

GRAND-CSL12_DLL16C serves as a crystallographic analog for TRIL12_DLL16C (**See Supplementary Discussion**). To illustrate the effect of alternate chirality on the internal hydrophobic residues in the outer coordination spheres, the apo-(GRAND-CSL12_DLL16C)₃ is overlaid onto the known apo-

(CSL16C)₃ (**Supporting information Figure S7, a**). This figure compares a parent peptide that contains solely L-amino acids in the sequence to one with a single D-Leu substitution. Both of the peptides fold into parallel 3SCCs as predicted. Although they are different in length by one heptad, the α -helical backbones of the two structures are extremely similar (RMSD = 0.36). Intriguingly, there are no kinks in the helical backbones observed in apo-(GRAND-CSL12_DLL16C)₃ suggesting that the incorporation of a D-Leu does not disturb the coiled coil secondary structure. In the sixteenth position, the C_β carbons of the Cys residues of the apo-(GRAND-CSL12_DLL16C)₃ point toward the N-termini of



a) apo-(CSL16C)₃ (PDB code: 5K92)¹³, b) apo-(CSL16Pen)₃ (PDB code: 3H5F)¹², c) apo-(GRAND-CSL16CL19D₃)₃, d) apo-(GRAND-CSL12D₃LL16C)₃, e) Hg(II)₅Zn(II)_N(GRAND-CSL16CL30H)₃⁺ (PDB code: 5KB1)¹³, f) [Hg(II)]₅[Zn(II)(H₂O/OH)]_N(CSL9PenL23H)₃¹⁺ (PDB code: 3PBJ)²⁸, g) Hg(II)(GRAND-CSL16CL19D₃)₃ and h) Hg(II)(GRAND-CSL12AL16C)₃. Main chain atoms are shown as ribbon diagrams. Residue side chains are present as sticks. D-Leu in c), d) and g) are colored in red. Hg(II) atoms and observed waters are shown as big and small spheres, respectively.

Figure 6. Effect of D-Leu in the twelfth position above the metal site (sixteenth) in the 3SCC environment. a) Side-on and b) top-down views of the overlay between apo-(GRAND-CSL12D₃LL16C)₃ (red) and apo-(CSL16C)₃ (PDB code: 5K92, orange)¹³ structures showing the difference in C_β carbon positions between D-Leu (red sticks) and L-Leu (orange sticks). From top down view of the N-termini, c) and d) representing the packing comparison between D-Leu and L-Leu residues (shown as spheres) in apo-(GRAND-CSL12D₃LL16C)₃ and apo-(CSL16C)₃, respectively.

compared in **Figure 6**. It is obvious that 12D-Leu residues are more tightly packed than seen for 12L-Leu, causing greater steric

hindrance above the metal binding layer. This perturbation occurs because the D-configuration repositions the C_β atoms from directing toward the N-termini (in L-Leu) to the C-termini direction (**Figure 6, a and b**). This C_β deviation twists the positions of δ-methyl groups (C_{δ1}, C_{δ2}) toward the center of the coiled coil. In the apo-(CSL16C)₃ structure, only one of the two δ-methyl atoms of each L-Leu residue is pointed toward the center, while the other points to the helical interface, thus opening up more space above the metal binding site and potentially making it less well-packed compared to 12D-Leu (**Figure 6, c and d**). This D-Leu effect shortens the separation between 12D-Leu and 16Cys layer to 2.32 Å as compared to the 4.92 Å observed in the apo-(CSL16C)₃ (**Figure 5**). The differential orientations of leucine layer in the outer coordination spheres, therefore, could represent an important effect of the amino acid side chains chirality on metal structures and binding mode preferences in the metallated-forms.

One may compare the known Hg(II)₅Zn(II)_N(GRAND-CSL16CL30H)₃⁺ to apo-(GRAND-CSL12D₃LL16C)₃ to obtain insight on Cd(II) complexation. As expected, the GRAND-CSL16CL30H is predisposed toward Hg(II)-binding as described above for CSL16C (**Supporting information Figure S10**).¹³ The metal induces significant rotation of the interior Cys

the helices and the S_γ atoms adopt two conformations (**Supporting information Figure S8**). The major Cys rotamers have the thiols positioned toward the metal binding core of the peptide, exhibiting a similar range of torsion angles with the apo-(CSL16C)₃ (-68.57° versus -66.24°) (**Supporting information Figure S8, b**). The S_γ-S_γ distances are comparable between both structures; 3.22 Å in apo-(GRAND-CSL12D₃LL16C)₃ and 3.32 Å (average) in apo-(CSL16C)₃ (**Supporting information Figure S9, a and b**). The minor Cys orientations of apo-(GRAND-CSL12D₃LL16C)₃ point their thiol groups to the outer interface, subsequently causing a long S_γ-S_γ separation (5.93 Å) between minor Cys conformers, which are not suitable for metal binding (**Supporting information Figure S8, c**). According to this first structural analysis of the layer at the sixteenth position, it appears that the apo-structures of (GRAND-CSL12D₃LL16C)₃ and (CSL16C)₃ present a relatively similar metal binding environment. The effect of D-Leu above the metal site is pronounced at the twelfth position. The packing of 12D-Leu residues in apo-(GRAND-CSL12D₃LL16C)₃ and 12L-Leu in apo-(CSL16C)₃ are

Figure 5. Interlayer spaces around the thiolate site of designed peptides.

conformations by moving the thiols downward and to the side. This shift orients the cysteine sulfur atoms more toward the helical interface leading to an expansion of S_γ-S_γ separations from 3.22 to 4.08 Å. The χ₁ dihedral angle changes from -66.24° (average) in the apo-structure to -150.35° (average). Unsurprisingly, the orientation of 12D-Leu in apo-(GRAND-CSL12D₃LL16C)₃ differs from the 12L-Leu in Hg(II)₅Zn(II)_N(GRAND-CSL16CL30H)₃⁺. First, both δ-methyl groups of each D-Leu residue, point toward the core of the helices, whereas in Hg(II)₅Zn(II)_N(GRAND-CSL16CL30H)₃⁺ only one of the C_δ atoms (C_{δ1}) of each 12L-Leu is in the core while the other is facing out toward the helical interface as shown in **Supporting Information Figure S11, a and b**. Moreover, the analysis of the aligned structures demonstrates that the C_β atoms of D-Leu are drastically different in position from the L-chirality, causing the C_{δ2} atoms in the D-Leu layer to tuck toward the center and move closer to the observed water in Hg(II)₅Zn(II)_N(GRAND-CSL16CL30H)₃⁺. This causes the 12D-Leu layer (C_{δ2} plane) to move closer to where the water would reside (only 1.30 Å distance), while the interior C_δ plane (C_{δ1}) of Hg(II)₅Zn(II)_N(GRAND-CSL16CL30H)₃⁺ is at a distance of 3.80 Å from the water (**Supporting Information Figure S11, c**). It is assumed that if the (GRAND-CSL12D₃LL16C)₃ were to bind a metal, the shift of the sulfur plane toward the binding would likely cause the layers (12D-Leu versus 16Cys) above the metal site to be separated by approximately 4.30 Å, while in the actual Hg(II)₅Zn(II)_N(GRAND-CSL16CL30H)₃⁺ structure the related distance determined from 12L-Leu is 5.92 Å. This strongly emphasizes that the D-Leu layer above the metal site is tightly-packed suggesting that the water should no longer exist within this tiny space. Therefore, steric encumbrance appears to be the basis for water exclusion in TRIL12D₃LL16C design.

Increasing the Coordination Number of Cd(II) By Modification of Outer Coordination Sphere Chirality: L-Leu to D-Leu Mutation on C-terminal Side

The combination of ^{113}Cd NMR, $^{111\text{m}}\text{Cd}$ PAC and EXAFS spectroscopies confirmed that the TRIL2WL16CL19_DL peptide binds Cd(II) with a higher coordination number than found for TRIL12_DLL16C with two species appearing in equal quantities as Cd(II)S₃(H₂O) and Cd(II)S₃(H₂O)₂.²⁵ Structural analysis of the apo-peptide is completed to evaluate hydrophobic packing in the absence of the metal site. The overlay of apo-(GRAND-CSL16CL19_DL)₃ with apo-(CSL16C)₃ illustrates that the α -helical backbones are well-aligned with no kinks observed in the D-Leu region (**Supporting information Figure S7, b**). The Cys residues of apo-(GRAND-CSL16CL19_DL)₃ display a single rotamer pointing toward the core of the structure resembling the major conformer of apo-(CSL16C)₃ and apo-(GRAND-CSL12_DLL16C)₃ (**Supporting information Figure S9**). This can be confirmed by their close values in side-chain torsion angles and S_i-S_j separations (**Table 2**). *The similarity in Cys layers reveals that*

the D-Leu does not affect the first coordination sphere ligands in the non-metallated form, regardless of the position where it is placed (12th or 19th position) in the outer coordination spheres. The effect of 19D-Leu is determined by overlaying the apo-(GRAND-CSL16CL19_DL)₃ onto the apo-(CSL16C)₃ structure. Both the 19D-Leu and the 19L-Leu side chains appear to direct the δ -methyl groups out toward the helical interface; however, the reorientation of the C _{β} atoms with the 19D-Leu in the apo-(GRAND-CSL16CL19_DL)₃ causes both of the δ -methylene groups to move further to the outer face than the 19L-Leu in apo-

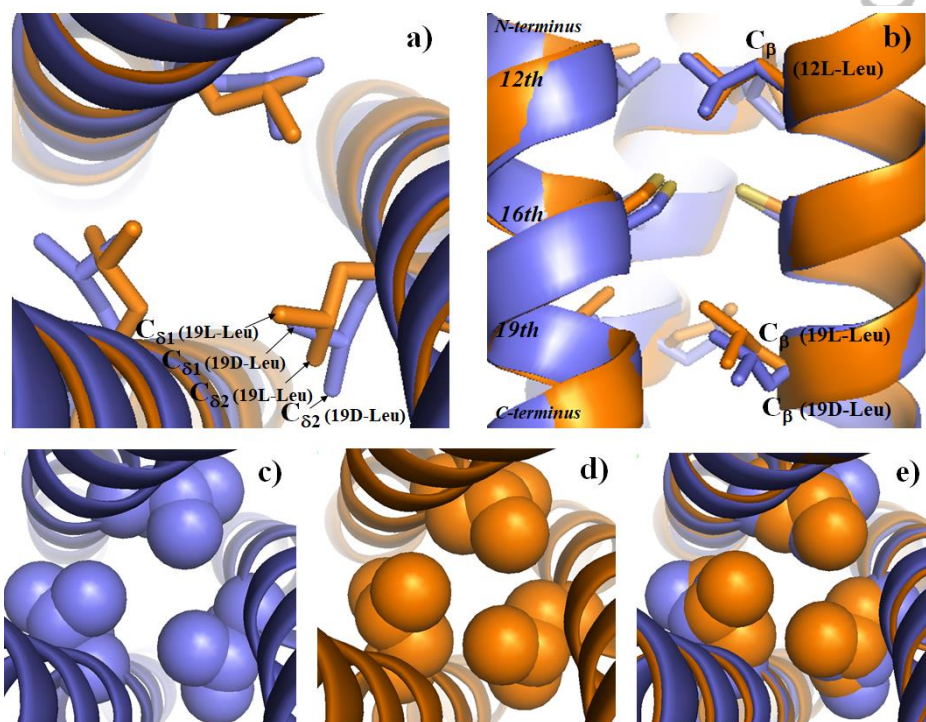


Figure 7. Effect of D-Leu in the nineteenth position below the metal site (sixteenth) in the 3SCC environment. Top panels: Overlays between apo-(GRAND-CSL16CL19_DL)₃ (blue) and apo-(CSL16C)₃ (PDB code: 5K92¹³, orange) structures demonstrate the deviation of a) C_β and b) C_γ positions of D-Leu (blue sticks) from L-Leu (orange sticks). Bottom panels: The packing in the nineteenth position of c) D-Leu (blue spheres) in apo-(GRAND-CSL16CL19_DL)₃ and d) L-Leu (orange spheres) in apo-(CSL16C)₃. In e) an overlay between c) and d).

(CSL16C)₃ (Figure 7, top panel). Moreover, the hydrophobic pocket below the metal site made by 19D-Leu appears to be bigger than 19L-Leu (Figure 7, bottom panel). Thus, the altered chirality of D-Leu can remove the steric constraints when it is placed below the metal site by rearranging the bulky δ-methyl groups away from the center of the coiled coil. Consequently, it generates more open space with the less-well-packed hydrophobes, which is believed to allow for better water access below the binding site. This conclusion is consistent with formation of the Cd(II)S₃(H₂O) corresponding to the ^{111m}Cd PAC angular frequency characteristics of 0.316 rad/ns.²⁵ As shown in the L16C variant, the cavity that lies between the 12L-Leu and 16Cys layers can bind Cd(II) from the top. Due to the limitation of spectroscopic techniques, these two conformations of Cd(II)S₃(H₂O) products (either with the water ligand positioned above or below) cannot be distinguished using the 0.316 rad/ns ^{111m}Cd PAC angular frequency value. In order to assess this model, the 12L-Leu packing in apo-(GRAND-CSL16CL19_DL)₃ is further investigated. If this hypothesis is true, the 12L-Leu in apo-(GRAND-CSL16CL19_DL)₃ should show sufficient space for water, comparable to the 12L-Leu layer in apo-(CSL16C)₃. The overlay structures of both apo-peptides (Figure 7) reveals that all

the C_β carbons in 12L-Leu are directed toward the N-termini due to their L-configuration. The 12L-Leu sidechains in apo-(GRAND-CSL16CL19_DL)₃ point one δ-methyl group toward the core, while the other is oriented more toward the helical interface. A similar observation is noted for the apo-(CSL16C)₃ parent

peptide. The packing in both structures look very similar even though the layer in apo-(GRAND-CSL16CL19_DL)₃ is slightly tighter-packed and the cavity is smaller (Supporting Information Figure S12). However, both structures generate a larger space above the metal site when compared to the smaller pocket made by the 12D-Leu in apo-(GRAND-CSL12_DLL16C)₃ (Figure 5). These crystal structures show that the cavity generated by the 12L-Leu in the apo-(GRAND-CSL16CL19_DL)₃ is large enough to house a water ligand above the metal site that can allow for Cd(II)S₃(H₂O) formation. Apparently, there are two spaces available in apo-(GRAND-CSL16CL19_DL)₃ for water access: one above that is likely partially occupied and a larger cavity below the

by the 12D-Leu in apo-(GRAND-CSL12_DLL16C)₃ (Figure 5). These crystal structures show that the cavity generated by the 12L-Leu in the apo-(GRAND-CSL16CL19_DL)₃ is large enough to house a water ligand above the metal site that can allow for Cd(II)S₃(H₂O) formation. Apparently, there are two spaces available in apo-(GRAND-CSL16CL19_DL)₃ for water access: one above that is likely partially occupied and a larger cavity below the metal site that could be fully occupied by solvent. Therefore, the observation of the 0.316 rad/ns angular frequency from ^{111m}Cd PAC could represent both 4-coordinate Cd(II) conformations where one has water bound on top with respect to the metal binding plane and the other has water bound below.

Apart from the 0.316 rad/ns angular frequency species observed in ^{111m}Cd PAC, another 50% of the products from TRIL2WL16CL19_DL was reported to exhibit a 0.159 rad/ns

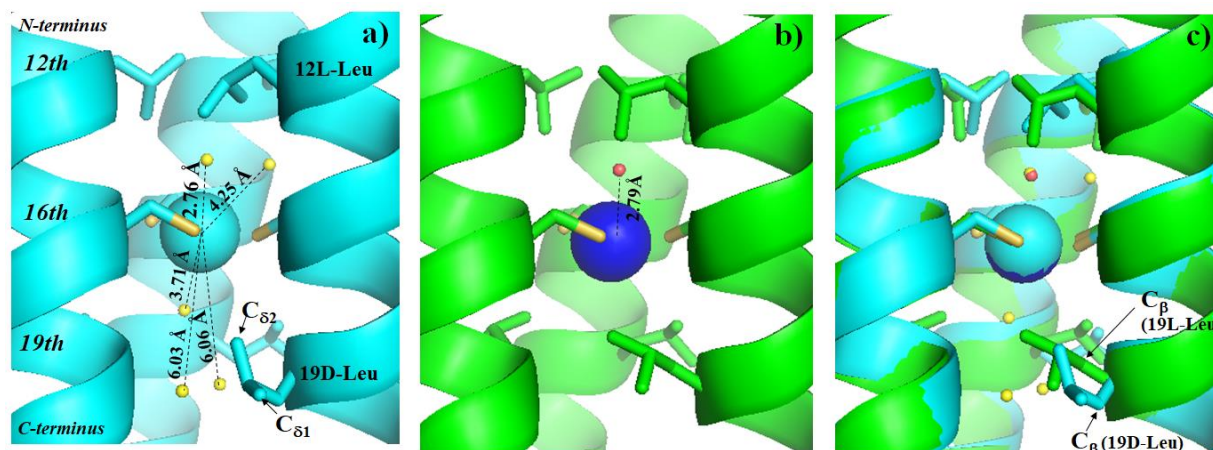


Figure 8. Side-on view of the metallated 3SCCs representing the existence of waters around the 16Cys coordinate site. In a) Hg(II)(GRAND-CSL16CL19_DL)₃, b) Hg(II)₅Zn(II)_N(GRAND-CSL16CL30H)₃⁺ (PDB code: 5KB1¹³) and c) an overlay between a) and b). Waters in Hg(II)(GRAND-CSL16CL19_DL)₃⁻ and Hg(II)₅Zn(II)_N(GRAND-CSL16CL30H)₃⁺ are shown as yellow and red small spheres, respectively. Hg(II) ions in Hg(II)(GRAND-CSL16CL19_DL)₃⁻ and Hg(II)₅Zn(II)_N(GRAND-CSL16CL30H)₃⁺ are represent in cyan and blue spheres, respectively. 12L-Leu, 16Cys (sulfurs=yellow) and 19D-Leu residues are shown as sticks with color corresponding to the ribbon diagram of each structure.

frequency that is uncommon in these designed peptide systems.²⁵ However, this lower frequency is consistent with a 5-

coordinate Cd(II)S₃(H₂O)₂ complex. Since the angular frequency is closer to zero, the NQI around the metal site is relatively symmetrical (where the perfect tetrahedral geometry ideally

shows ω_0 of 0 rad/ns).³⁷ Therefore, this 0.159 rad/ns value suggests an axially symmetric trigonal bipyramidal structure. As shown by the crystallography described above, the existence of two cavities above and below the metal site in the apo-(GRAND-CSL16CL19_DL)₃⁻ supports this possibility as space is available for waters to form a Cd(II)S₃(H₂O)₂ structure.

Excitingly, additional evidence supporting the possibility of simultaneous water access in this peptide has been obtained through the crystal structure of Hg(II)(GRAND-CSL16CL19_DL)₃⁻. Though the metal center is not Cd(II)-bound, the mercurocurated binding site reveals some interesting aspects related to the previous predictions. Five water molecules are observed within both cavities around the metal layer of Hg(II)(GRAND-CSL16CL19_DL)₃⁻ (**Figure 8a**). The first water is situated above the metal site, at a 2.76 Å distance from the Hg(II) center. This value is close to the previously observed water found in Hg(II)₅Zn(II)_N(GRAND-CSL16CL30H)₃⁺ (2.79 Å).¹³ It is stabilized by H-bonding interactions with Cys ligands and the second water which is located close to the helical interface between two helical chains of the 3SCC. The second water is 3.11 Å from the first water and 4.25 Å from the Hg(II) center. The reason this second water is observed in this Hg(II)(GRAND-CSL16CL19_DL)₃⁻ structure, but not in Hg(II)₅Zn(II)_N(GRAND-CSL16CL30H)₃⁺ is probably because Hg(II)(GRAND-CSL16CL19_DL)₃⁻ was crystallized in P2₁2₁2₁ space group which does not impose three fold symmetry on the helices. However, the R32 space group for Hg(II)₅Zn(II)_N(GRAND-CSL16CL30H)₃⁺ is tightly packed and the three-fold crystallographic symmetry constraints may exclude any waters which are not aligned on the three fold axis, thus resulting in the appearance of there being only one axial water positioned above the Hg(II) (**Figure 8b**). The third, fourth and fifth waters

are positioned within the nineteenth D-Leu cavity below the Cys plane with separations of 3.71 Å, 6.03 and 6.06 Å away from Hg(II), respectively. The third water is situated near one of the 3SCC helices above the C_{δ2} plane of the 19D-Leu, lying close to the helical interface and showing strong H-bonding interactions with the thiol and carbonyl oxygen of the 16Cys residue of the corresponding helix. Moreover, it is at a distance of 3.24 Å and 4.28 Å from the fourth and fifth waters, respectively that are situated toward the C-termini. The fourth water, is oriented more to the center of the helix, on the same plane as C_{δ1} atom of the 19D-Leu. The fifth water is H-bonded with the carbonyl oxygen of one of the 19D-Leu residues. These observations strongly suggests that once the metal is bound in the Cys plane in Hg(II)(GRAND-CSL16CL19_DL)₃⁻, the pocket made by the 19D-Leu is sufficiently large as to accommodate more than just one water molecule.

To analyze the impact of D-Leu on hydrophobic packing in the metallated structures further, the Hg(II)(GRAND-CSL16CL19_DL)₃⁻ is aligned to the previously published Hg(II)₅Zn(II)_N(GRAND-CSL16CL30H)₃⁺. **Figure 8c** represents an excellent overlay of the bound S_γ conformers between the two structures as confirmed from their similarity in χ_1 (**Table 3**). The Hg(II) ions of the two Hg(II)-structures are in the same plane (**Figure 8c**). The averaged Hg(II)-S distance in Hg(II)(GRAND-

CSL16CL19_DL)₃⁻ is 2.43 Å, which is close to the distances of trigonal planar Hg(II) structures in Hg(II)₅Zn(II)_N(GRAND-CSL16CL30H)₃⁺ and reported small molecule complexes.^{14,15,38} As previously noted, all the waters observed in the outer coordination spheres of Hg(II)-bound structures are non-bonded and are believed to have H-bond interactions to the bound Cys ligands, which helps compensate the negative charge of the metallated site. **Figure 5 (e and g)** confirms that the interlayer space above the metal site in Hg(II)(GRAND-CSL16CL19_DL)₃⁻ is slightly bigger than Hg(II)₅Zn(II)_N(GRAND-CSL16CL30H)₃⁺ due to the presence of the second water above the metal containing layer that is located near the helical interface between two of the helical chains. The

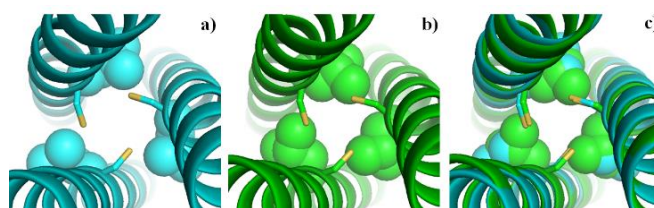


Figure 9. Packing comparison of hydrophobic residues around the metal site between Hg(II)(GRAND-CSL16CL19_DL)₃⁻ and Hg(II)₅Zn(II)_N(GRAND-CSL16CL30H)₃⁺ (PDB code: 5KB1)¹³. Packing of residues in the nineteenth position below the metal site, a) 19D-Leu of Hg(II)(GRAND-CSL16CL19_DL)₃⁻, b) 19L-Leu of Hg(II)₅Zn(II)_N(GRAND-CSL16CL30H)₃⁺ and c) an overlay between a) and b), which emphasizes the similarity of the bound S_γ conformers (sticks) in the sixteenth position from the top-down view (Hg(II) ions and observed waters of both structures are omitted for clarity.) Main chain atoms are represent as ribbon diagrams, 16Cys as sticks, D-Leu and L-Leu as spheres.

axial water observed directly on top of the Hg(II) atom in Hg(II)(GRAND-CSL16CL19_DL)₃⁻ is within 0.10 Å of the position of water observed in Hg(II)₅Zn(II)_N(GRAND-CSL16CL30H)₃⁺ (**Figure 8c**). While the hydrophobicity of the layer at the twelfth positions are slightly different, both metallated-structures easily accommodate a water molecule axially above the Hg(II). Moreover, due to the low symmetry requirement of P2₁2₁2₁ space group, the cavity above the metal site in Hg(II)(GRAND-CSL16CL19_DL)₃⁻ is also amenable for a second water to H-bond with the centrally axial water. These structural comparisons confirm that the space in the layer at the 12th position is suitable for water access, demonstrating that the Cd(II)S₃(H₂O) species with a water ligand oriented toward the N-terminus in TRIL2WL16CL19_DL is reasonable. The significant change in leucine orientations in the layer at the nineteenth position strongly suggests that the 19L-Leu layer in Hg(II)₅Zn(II)_N(GRAND-CSL16CL30H)₃⁺ packs tighter than the 19D-Leu in Hg(II)(GRAND-CSL16CL19_DL)₃⁻ (**Figure 9**). It is obvious that the C_β deviation of D-Leu forces the whole side chain to be directed more toward the helical interface, generating a larger interlayer space below the metal site compared to the Hg(II)₅Zn(II)_N(GRAND-CSL16CL30H)₃⁺. The alignment of both structures demonstrates that the tighter 19L-Leu packing in the metallated-L16C peptide would cause drastic steric clashes if waters were to be present as similar to the Hg(II)(GRAND-CSL16CL19_DL)₃⁻. This not only explains the

reasons why the altered D-Leu side chain removes the steric hindrance below the metal binding site, allowing for more water access in TRIL2WL16CL19_DL, but also hints to why there is no observation of water below the metal binding site that could bind to Cd(II) when the 19L-Leu configuration is placed in the TRIL16C peptide.

Conclusion

One of the most challenging aspects of *de Novo* metalloprotein design is developing strategies to control coordination geometry within a protein environment. To achieve this objective, one must not only understand the positioning of first coordination sphere ligands, but also comprehend what features of the outer coordination spheres are necessary to obtain a desired geometry. We have used correlated X-ray crystallographic structures of Hg(II)-peptide complexes to evaluate how steric changes in either the first or second coordination sphere influence the coordination numbers of Cd(II) complexes in 3SCC environments. In some ways, the results are surprising in that they illustrate that a well-reasoned modification may achieve the desired structural result, but for reasons that might not have originally been predicted. An example of this is the ability to control water access to the metal. Clearly, sterics of second coordination sphere side chains influence the available space around the metal site. The predisposition of Cys upon trigonal planar binding allows for an expansion of the interlayer space between the Leu layer (above) and the metal site. The presence of a water molecule in such a cavity of the metallated structure strongly suggests that Cd(II)S₃O formation is possible when Cd(II) is bound to the L16C peptide. However, the fourth ligand is only available at a significant price due to the strong hydrophobicity of Leu residues above the metal site. As a consequence, a mixture of 3- and 4-coordinate Cd(II) is formed. The shift to 100% 3-coordinate Cd(II)S₃ can be achieved by reducing the space for water above the metal site. This can be done in two ways. Exploiting the chirality of D-Leu, one can reorient, or “lower”, the hydrophobic side chain toward the metal binding plane while keeping the Cd(II) at the relatively same position within the helical scaffold. As predicted, structural analysis confirms that D-Leu side chains are reoriented toward the C-termini of the structure, causing steric interference above the metal site. However, the second approach, use of Pen ligand to perturb the first coordination sphere ligand, achieves the same objective by an unpredicted structural change. The bulky Pen restricts thiol rotation, causing a shift in the metal plane towards the Leu layer above the site, thus “raising” the metal binding sulfur layer and the Cd(II) towards the N-termini, which blocks water access. Therefore in the D-Leu case, the roof above the metal site is lowered, whereas in the second substitution with Pen, the floor containing the metal is raised. Both effects diminish space for solvation of the Cd(II) center, generating a pure Cd(II)S₃.

In contrast, when the size of the leucine side chain is diminished with alanine, a larger space is generated, which allows for four waters to occupy the newly formed cavity.

Moreover, the structural analysis confirms that the position of D-Leu in the outer coordination spheres generates a different steric effect on the metal site, as this lowers the bulky isopropyl groups of L-leucine away from the metal center. The consequence of this change is a trigonal bipyramidal Cd(II) because two cavities are simultaneously available above and below the binding site. These studies provide insights on how to control desired metal geometries in proteins, which are potentially useful for broader applications in future metalloprotein designs.

Experimental Section

Materials: Fmoc-protected amino acids and the MBHA rink amide resin were purchased from Novabiochem; *N*-hydroxybenzotriazole (HOBt) and 2-(1H-benzotriazol-1-yl)-1,1,3,3-tetramethyluronium hexafluorophosphate (HBTU) were bought from Anaspec Inc.; diisopropylethylamine (DIEA), acetic anhydride, and pyridine were purchased from Aldrich; piperidine was supplied by Sigma; and *N*-methylpyrrolidinone (NMP) and *N,N*-dimethylformamide (DMF) were obtained from Fisher Scientific.

Peptide synthesis and purification: All peptide variants were synthesized on an Applied Biosystems 433A automated peptide synthesizer with Fmoc-protected amino acids using the standard Fmoc protocol (Applied Biosystems).³⁹ The C-terminus of the peptides was amidated on the solid support MBHA rink amide resin (0.25 mmole scale) with HBTU/HOBt/DIEA coupling methods. The N-terminus was acetylated with a solution of 4% (v/v) acetic anhydride, 4.3% (v/v) pyridine, and 91.7% *N,N*-dimethylformamide (DMF). The peptides were cleaved from the resin using a cleavage mixture of 90% trifluoroacetic acid (TFA), 5% anisole, 3% thioanisole, and 2% ethanedithiol for 3.5 hours. The cleaved peptide solution was filtered and evaporated under a dry N₂-flow until a glassy film appeared on the surface. Cold diethyl ether was then added to the thin film to obtain a precipitated white crude peptide. This crude was re-dissolved in ddH₂O and lyophilized to get a fluffy white powder, which was subsequently dissolved in 10% acetic acid. The peptide was purified by reversed phase HPLC on a Waters 600 Semiprep HPLC peptide C-18 using a linear gradient of 0.1% TFA in water to 0.1% TFA in 9:1 CH₃CN/H₂O program over 30 mins (flow rate 10 mL/min). The purified peptides were identified by electrospray mass spectrometry. Concentration of peptide stock solutions was determined by quantitation of the cysteine thiols using Ellman's test, which uses dithionitrobenzoate (DTNB) as an indicator.⁴⁰

Crystallizations: All peptides were crystallized by sitting drop vapor diffusion experiments at 20 °C with drops containing equal volumes of peptide (0.75 μL) and precipitant (0.75 μL) solutions. The Hg(II)(GRAND-CSL12A16C)₃⁻ crystals were prepared from a peptide solution (20 mg/mL GRAND-CSL12A16C, 0.92 eq of HgCl₂ per 3SCC peptide, 15 mM Zn(OAc)₂ and 0.5 mM Tris buffer pH 8.5) and a well solution (0.1 M MES pH 6.5 and 25% (w/v) PEG-1000). The apo-GRAND-CSL12_DLL16C was grown from 20 mg/mL GRAND-

CSL12_DLL16C, 15 mM Zn(OAc)₂ and 0.5 mM Tris buffer pH 8.5. The precipitant solution contains 40% (v/v) PEG-400, sodium acetate buffer pH 4.5 at a final well solution pH 5.4. The apo-GRAND-CSL16CL19_DL solution was prepared from 20 mg/mL peptide, 15 mM Zn(OAc)₂ and 0.5 mM Tris buffer pH 8.5. The well solution contains 25% (v/v) PEG-2000 MME and 0.1 M MES pH 6.5. The crystals of Hg(II)GRAND-CSL16CL19_DL were crystallized from a peptide solution (20 mg/mL GRAND-CSL16CL19_DL, 0.92 eq of HgCl₂ per 3SCC peptide, 15 mM Zn(OAc)₂ and 0.5 mM Tris buffer pH 8.5) against well solution (0.2 M Lithium acetate and 20% (v/v) PEG-3350). Crystals were cryoprotected in a mother liquor containing 20% glycerol prior to supercooling in liquid N₂ for data collection.

Data collections and refinements: Data were collected at the Advanced Photon Source of the Argonne National Laboratory on the LS-CAT Beamline 21-ID-F, equipped with a Mar 225 CCD detector, respectively. All data were collected with a 1° oscillation then processed and scaled with HKL2000.⁴¹ All structures presented were solved by molecular replacement using Molrep⁴² in the CCP4 suite of programs⁴³⁻⁴⁶, then underwent iterative rounds of electron density fitting and refining in Coot⁴² and Buster 2.11.2 program⁴⁷, respectively. The X-ray crystal structures of well-folded, three-stranded parallel coiled coil peptides of apo-(GRAND-CSL12_DLL16C)₃, apo-(GRAND-CSL16CL19_DL)₃ and Hg(II)(GRAND-CSL16CL19_DL)₃⁻ were determined to 1.34 Å, 1.83 Å and 1.93 Å resolution, respectively. The crystallographic data for the crystal structures is shown in **Table 3**. The apo-(GRAND-CSL12_DLL16C)₃ crystallized in the space group R32, contains one single strand of peptide per asymmetric unit with a Matthew's coefficient of 2.38 corresponding to 47.67% solvent content. The three stranded coiled coil is obtained by the combination of three adjacent symmetric units that are crystallographic imposed by the three-fold axis. The structure was solved using a previously published method.⁴⁸ The structure was refined to 1.42 Å (R_{working} = 19.6%, R_{free} = 20.3 %).

Sharing similar lattice packing of the R32 space group, the refined apo-(GRAND-CSL12_DLL16C) was subsequently employed to be a search model for apo-(GRAND-

CSL16CL19_DL) by mutating the 12 D-Leu to L-Leu. 19 D-Leu was replaced after the first round of refinement. The solvent content per asymmetric unit of this structure is 48.60%. The structure was refined to 1.83 Å (R_{working} = 20.0%, R_{free} = 20.6%). The helix of Hg(II)(GRAND-CSL12A16C)₃⁻ was solved by a GRAND-CSL12A16C model from the previously published Zn(II)(GRAND-CSL12A16C)₃⁻. The structure was refined to 1.93 Å (R_{working} = 23.14%, R_{free} = 25.15 %). The Hg(II)(GRAND-CSL16CL19_DL)₃⁻, assigned to space group P2₁2₁, was solved using AutoSol Wizard in Phenix.⁴⁹⁻⁵¹ To solve the structure, the anomalous difference of heavy atoms, Hg(II) and Zn(II), was determined to generate the experimental phases. The obtained solution reveals a possible three-stranded coiled coil packing per asymmetric unit, yet the third strand was broken in the middle, missing the residues 19Leu, 20Glu, 21Lys and 22Lys. By using the 2F_o-F_c electron density as a guide, all missing residues were built back into the chain to generate the final starting model which consequently served as the search model in MolRep(reference). D-Leu at the nineteenth position was replaced with L-Leu after one round of refinement according to the difference density shown in the F_o-F_c map. The Matthew's coefficient is 4.68 corresponding to 73.74% solvent. The structure was refined to 1.84 Å (R_{working} = 21.1%, R_{free} = 22.6 %). The validity of the models were verified using the MolProbity software.⁵² All non-glycine residues of these structures fall in the preferred right handed α-helical region of the Ramachandran plot. Every side chain is present in the preferred rotameric conformation.

Table 3: Data collection and refinement statistics of the crystal structures

Peptides	apo-(GRAND-CSL12 _D LL16C) ₃ PDB code: 6EGL	apo-(GRAND-CSL16CL19 _D L) ₃ PDB code: 6EGM	Hg(II)(GRAND-CSL12A16C) ₃ ⁻ PDB code: 6EGO	Hg(II) (GRAND-CSL16CL19 _D L) ₃ ⁻ PDB code: 6EGN
Data collection				
SpaceGroup	R32	R32	R32	P2 ₁ 2 ₁
Cell dimensions				
a, b, c (Å)	38.213, 38.213, 140.655	37.898, 37.898, 140.667	38.186, 38.186, 142.385	
α, β, γ (°)	90.00, 118.78, 90.00	90.00, 90.00, 120.00	90.00, 90.00, 120.00	2.636, 80.508, 88.730 90.00, 90.00, 90.00
Wavelength (Å)	0.97872	0.97872	0.98756	0.98756
Resolution (Å) ¹	1.42(1.42-1.40)	1.83 (1.87-1.83)	1.84 (1.87-1.84)	1.84 (1.87-1.84)
R _{sym} (%) ²	5.6 (43.4)	9.4 (48.3)	6.9 (54.4)	12.9 (60.8)

$\langle I/\sigma \rangle^3$	>50 (2)	>50 (2)	> 50 (2)	>50 (2)
Completeness (%) ⁴	99.3 (100)	99.4 (100)	98.6 (100)	97.6 (99.6)
Redundancy	5.6 (5.5)	35.6 (39.8)	15.8 (12.4)	8.3 (7.6)
Refinement				
Resolution (Å)	1.42	1.83	1.92	1.84
R-Factor (%) ⁵	19.6	20.0	23.1	21.1
R _{free} (%) ⁶	20.3	20.6	25.1	22.6
Protein atoms	302	273	318	870
Metal ions	1 Zn(II)	1 Zn(II)	1/3 Hg(II) 1 Zn(II) on surface	1 Hg(II) 3 Zn(II)
Water Molecules	52	44	29	189
Unique Reflections	8093	2584	3266	20219
R.m.s.d.⁷				
Bonds	0.01	0.01	0.06	0.01
Angles	1.15	1.01	0.685	1.08
MolProbity Score ⁸	1.11	0.50	1.25	1.45
Clash Score ⁸	3.17	0.00	3.09	4.20

¹Statistics for highest resolution bin of reflections in parentheses

² $R_{\text{sym}} = \sum_h \sum_j |I_{hj} - \langle I_h \rangle| / \sum_h \sum_j I_{hj}$, where I_{hj} is the intensity of observation j of reflection h and $\langle I_h \rangle$ is the mean intensity for multiply recorded reflections.

³Intensity signal-to-noise ratio

⁴Completeness of the unique diffraction data

⁵R-factor = $\sum_h ||F_o| - |F_c|| / \sum_h |F_o|$, where F_o and F_c are the observed and calculated structure factor amplitudes for reflection.

⁶R_{free} is calculated against a 10% random sampling of the reflections that were removed before structure refinement.

⁷Root mean square deviation of bond lengths and bond angles

⁸Reference 52

Acknowledgements

V.L.P. and L.R. thank the National Institutes of Health for support of this research (ES012236), and J.A.S. is supported by the University of Michigan Center for Structural Biology. L.R. thanks Dr. Jennifer Meagher for data collections, the CCP4/APS School in Macromolecular Crystallography: from data collection to structure refinement and beyond 2016 for their help on crystal structure solution process and the Royal Thai Government and the Skill Development Grant from King Mongkut's University of

Technology, Thonburi, Thailand for funding. Use of the Advanced Photon Source, an Office of Science User Facility operated for the U.S. Department of Energy (DOE) Office of Science by Argonne National Laboratory, was supported by the U.S. DOE under contract no. DE-AC02-06CH11357. Use of the LS-CAT Sector 21 was supported by the Michigan Economic Development Corporation and the Michigan Technology Tri-Corridor (Grant 085P1000817).

Accession Codes

apo-(GRAND-CSL12_DLL16C)₃, PDB ID: 6EGL
 apo-(GRAND-CSL16CL19_DL)₃, PDB ID: 6EGM
 Hg(II)(GRAND-CSL16CL19_DL)₃⁻, PDB ID: 6EGN
 Hg(II)(GRAND-CSL12AL16C)₃⁻, PDB ID: 6EGO

References

- (1) G. R. Dieckmann, D. K. McRorie, J. D. Lear, K. A. Sharp, W. F. DeGrado, V. L. Pecoraro, *J. Mol. Biol.* **1998**, 280 (5),

- 897-917.
- (2) G. R. Dieckmann, D. K. Mcrorie, D. L. Tierney, L. M. Utschig, C.P. Singer, T. V. O'Halloran, J. E. Penner-Hahn, W. F. Degrado, V. L. Pecoraro, *J. Am. Chem. Soc.* **1997**, *119* (4), 6195-6196.
- (3) V. L. Pecoraro, A. F. A. Peacock, O. Iranzo, Ł. Marek, In *Bioinorganic Chemistry*; Long, E., Eds.; ACS Symposium Series: American Chemical Society, Washington DC, **2009**, 183-197.
- (4) B. T. Farrer, C. P. McClure, J. E. Penner-Hahn, V. L. Pecoraro, *Inorg. Chem.* **2000**, *39* (24), 5422-5423.
- (5) B. T. Farrer, V. L. Pecoraro, *Proc. Natl. Acad. Sci. U.S.A.* **2003**, *100* (7), 3760-3765.
- (6) M. Matzapetakis, B. T. Farrer, T.-C. Weng, L. Hemmingsen, J. E. Penner-Hahn, V. L. Pecoraro, *J. Am. Chem. Soc.* **2002**, *124* (27), 8042-8054.
- (7) M. Matzapetakis, D. Ghosh, T.-C. Weng, J. E. Penner-Hahn, V. L. Pecoraro, *J. Biol. Inorg. Chem.* **2006**, *11* (7), 876-890.
- (8) O. Iranzo, S. Chakraborty, L. Hemmingsen, V. L. Pecoraro, *J. Am. Chem. Soc.* **2011**, *133* (2), 239-251.
- (9) O. Iranzo, P. W. Thulstrup, S.-B. Ryu, L. Hemmingsen, V. L. Pecoraro, *Chemistry* **2007**, *13* (33), 9178-9190.
- (10) D. S. Touw, C. E. Nordman, J. A. Stuckey, V. L. Pecoraro, *Proc. Natl. Acad. Sci. U.S.A.* **2007**, *104* (29), 11969-11974.
- (11) S. Chakraborty, D. S. Touw, A. F. A. Peacock, J. A. Stuckey, V. L. Pecoraro, *J. Am. Chem. Soc.* **2010**, *132* (38), 13240-13250.
- (12) A. F. A. Peacock, J. A. Stuckey, V. L. Pecoraro, *Angew. Chem. Int. Ed. Engl.* **2009**, *48* (40), 7371-7374.
- (13) L. Ruckthong, M. L. Zastrow, J. A. Stuckey, V. L. Pecoraro, *J. Am. Chem. Soc.* **2016**, *138* (36), 11979-11988.
- (14) E. S. Gruff, K. S. Koch, *J. Am. Chem. Soc.* **1990**, *112*, 1245.
- (15) G. Christou, K. Folting, J. C. Huffman, *Polyhedron* **1984**, *3*, 1243-1247.
- (16) K.-H. Lee, M. Matzapetakis, S. Mitra, E. N. G. Marsh, V. L. Pecoraro, *J. Am. Chem. Soc.* **2004**, *126* (30), 9178-9179.
- (17) K.-H. Lee, C. Cabello, L. Hemmingsen, E. N. G. Marsh, V. L. Pecoraro, *Angew. Chem. Int. Ed. Engl.* **2006**, *45* (18), 2864-2868.
- (18) O. Iranzo, D. Ghosh, V. L. Pecoraro, *Inorg. Chem.* **2006**, *45* (25), 9959.
- (19) D. Ghosh, V. L. Pecoraro, *Inorg. Chem.*, **2004**, *43*, 7902-7915.
- (20) O. Iranzo, T. Jakusch, K.-H. Lee, P. W. Thulstrup, L. Hemmingsen, V. L. Pecoraro, *Chem: Eur. J.* **2009**, *15*, 3761-3772.
- (21) M. Matzapetakis, V. L. Pecoraro, *J. Amer. Chem. Soc.* **2005**, *127* (51): 18229-18233.
- (22) M. Stachura, S. Chakraborty, A. Gottberg, L. Ruckthong, V. L. Pecoraro, L. Hemmingsen, *J. Amer. Chem. Soc.*, **2017**, *139*, 79-82.
- (23) A. F. A. Peacock, O. Iranzo, V. L. Pecoraro, *Dalton Transactions*, **2009**, 2271- 2280.
- (24) A. F. A. Peacock, L. Hemmingsen, V. L. Pecoraro, *Proc. Natl. Acad. Sci. U.S.A.* **2008**, *105* (43), 16566-16571.
- (25) L. Ruckthong, A. Deb, L. Hemmingsen, J. E. Penner-Hahn, V. L. Pecoraro, V. L. *J. Biol. Inorg. Chem.* **2018**, *23* (1), 123-135.
- (26) L. Ruckthong, Crystallographic Comparison of Tris-thiolate Sites in Designed Proteins to Control Metal Geometries. Ph.D. Dissertation. University of Michigan, Ann Arbor, MI, USA, **2016**.
- (27) B. Lovejoy, S. Choe, D. Cascio, D. K. Mcrorie, F. William, D. Eisenberg, W. F. Degrado, *Science* **1993**, *259* (5099), 1288-1293.
- (28) M. L. Zastrow, A. F. A. Peacock, J. A. Stuckey, J. A.; V.L. Pecoraro, *Nat. Chem.* **2011**, *4*, 118-123.
- (29) L. Ruckthong, A. F. A. Peacock, C. E. Pascoe, L. Hemmingsen, J. A. Stuckey, V. L. Pecoraro, *Chemistry* **2017**, *23* (34), 8232-8243.
- (30) E. Khazina, V. Truffault, R. Büttner, S. Schmidt, M. Coles, O. Weichenrieder, *Nat. Struct. Mol. Biol.* **2011**, *18* (9), 1006.
- (31) E. Khazina, O. Weichenrieder, *Proc. Natl. Acad. Sci. U.S.A.* **2009**, *106* (3), 731.
- (32) E. Khazina, O. Weichenrieder, *Elife* **2018**, *7*, 1.
- (33) S. Geremia; L. Di Costanzo; L. Randaccio; D.E. Engel; A. Lombardi; F. Nistri; W.F. DeGrado, *J. Am. Chem. Soc.*, **2005**, *127*(49), 17266-17276.
- (34) W.F. DeGrado; L. Di Costanzo; S. Geremia; A. Lombardi; V. Pavone; L. Randaccio, *Angew Chem Int Ed Engl.*, **2003**, *42*(4), 417-420.
- (35) L. Di Costanzo; H. Wade; S. Geremia; L. Randaccio; V. Pavone; W.F. DeGrado; A. Lombardi, *J. Am. Chem. Soc.*, **2001**, *123* (51), 12749-12757.
- (36) P. B. Harbury, T. Zhang, P. S. Kim, T. Alber, *Science* **1993**, *262* (5138), 1401-1406
- (37) L. Hemmingsen, *Encycl. Inorg. Bioinorg. Chem.* **2011**, 1-17.
- (38) S. P. Watton, J. G. Wright, F. M. MacDonnell, J. W. Bryson, M. Sabat, T. V. O'Halloran, *J. Am. Chem. Soc.* **1990**, *112*, 2824-2826.
- (39) W. C. Chan, P. D. White, ed., *Fmoc Solid Phase Peptide Synthesis: A Practical Approach*; Oxford University Press: New York, **2000**.
- (40) G. L. Ellman, *Arch. Biochem. Biophys.* **1959**, *82*, 70-77.
- (41) Z. Otwinowski, W. Minor, *Methods Enzymol.* **1997**, *276*, 307-326.
- (42) A. Vagin, A. Teplyakov, *Acta Crystallogr D: Biol Crystallogr* **2010**, *66*, 22-25.
- (43) M. D. Winn, C. C. Ballard, K. D. Cowtan, E. J. Dodson, P. Emsley, P. R. Evans, R. M. Keegan, E. B. Krissinel, A. G. W. Leslie, A. McCoy, S. J. McNicholas, G. N. Murshudov, N. S. Pannu, E. A. Potterton, H. R. Powell, R. J. Read, A. Vagin, K. S. Wilson, *Acta Crystallogr. Sect. D: Biol. Crystallogr.* **2011**, *67* (4), 235-242.
- (44) E. Potterton, P. Briggs, M. Turkenburg, E. Dodson, *Acta*

- Crystallogr. Sect. D Biol. Crystallogr.* **2003**, *59* (7), 1131-1137.
- (45) A. J. McCoy, R. W. Grosse-Kunstleve, P. D. Adams, M. D. Winn, L. C. Storoni, R. J. Read, *J. Appl. Crystallogr.* **2007**, *40* (4), 658-674.
- (46) P. Emsley, K. Cowtan, *Acta Crystallogr D: Biol Crystallogr* **2004**, *60*, 2126-2137.
- (47) G. Bricogne, E. Blanc, M. Brandl, C. Flensburg, P. Keller, W. Paciorek, P. Roversi, A. Sharff, A., O.S. Smart, C. Vonrhein, T. O. Womack, *BUSTER version 2.11.2*; United Kingdom: Global Phasing Ltd: Cambridge, UK.
- (48) L. Ruckthong, J. A. Stuckey, V. L. Pecoraro, V. L. *Method Enzym.* **2016**, *580*, 135-148.
- (49) T. C. Terwilliger, P. D. Adams, R. J. Read, A. J. McCoy, N. W. Moriarty, R. W. Grosse-Kunstleve, P. V. Afonine, P. H. Zwart, L. W. Hung, *Acta Crystallogr D: Biol Crystallogr* **2009**, *65*, 582-601.
- (50) T. C. Terwilliger, *Acta Crystallogr D: Biol Crystallogr* **2000**, *56*, 965-972.
- (51) R. W. Grosse-Kunstleve, P. D. Adams, *Acta Crystallogr D: Biol Crystallogr* **2003**, *59*, 1966-1973.
- (52) V. B. Chen, W. B. Arendall, J. J. Headd, D. A. Keedy, R. M. Immormino, G. J. Kapral, L. W. Murray, J. S. Richardson, D. C. Richardson, *Acta Crystallogr., Sect. D: Biol. Crystallogr.* **2010**, *66*(1), 12-21.

TOC Figure

